Supramolecular Ordering, Thermal Behavior, and Photophysical, Electrochemical, and Electroluminescent Properties of Alkoxy-Substituted Yne-Containing Poly(phenylene-vinylene)s

ARTICLE *in* MACROMOLECULES · SEPTEMBER 2004

Impact Factor: 5.8 · DOI: 10.1021/ma0488111

Supramolecular Ordering, Thermal Behavior, and Photophysical, Electrochemical, and Electroluminescent Properties of Alkoxy-Substituted Yne-Containing Poly(phenylene−vinylene)s

Daniel Ayuk Mbi Egbe,*,† Benjamin Carbonnier,‡ Liming Ding,§ David Mühlbacher,⊥ Eckhard Birckner,|| Tadeusz Pakula,*,‡ Frank E. Karasz,§ and Ulrich-Walter Grummt||

Institut für Organische Chemie und Makromolekulare Chemie der Friedrich-Schiller Universität Jena, Humboldtstrasse 10, D-07743 Jena, Germany, Max-Planck-Institut für Polymerforschung, Ackermannweg 10, D-55128 Mainz, Germany, Department of Polymer Science and Engineering, University of Massachusetts, Amherst, Massachusetts 01003, Konarka Austria Forschungs-u. Entwicklungs GmbH, Gruberstrasse 40−42, A-4010 Linz, Austria, and Institut für Physikalische Chemie der Friedrich-Schiller Universität Jena, Lessingstrasse 10, D-07743 Jena, Germany

Received June 16, 2004; Revised Manuscript Received July 17, 2004

ABSTRACT: Alkoxy-substituted and defect-free yne-containing poly(phenylene−vinylene)s, **15a**−**d**, having the general constitutional unit (−Ph−C≡C−Ph−CH=CH−Ph−CH=CH−)$_n$ synthesized through the olefination reactions of the fluorophoric dialdehyde **7** [1,2-bis(4-formyl-2,5-dialkoxyphenyl)acetylene] with various 2,5-dialkoxy-*p*-xylylenebis(diethylphosphonates), **14a**−**d**, are reported. A new synthetic route to 1-bromo-2,5-dialkoxybenzaldehyde (starting material for the synthesis of **7**) allowing the grafting of all types of alkoxy side chains is also reported. Bulk state properties of the four polymeric materials have been analyzed using various experimental methods giving information on the thermal behavior as well as self-assembling morphologies at different size scales. Crystalline superstructures of either spherulitic or rodlike morphology, comprised of polymeric backbone layers separated by the side chains are identified to develop by nucleation and growth process for symmetrically alkoxy substituted **15a**−**c**. Discrepancy between optical (E_g^{opt}) and electrochemical (E_g^{ec}) band gaps was observed to be dependent on the bulkiness (**15c**) and length (**15b**) of the grafted side chains. Octadecyloxy side chains in **15b** not only lead to well structured photoluminescence and electroluminescence spectra and higher fluorescence quantum yields but also allow the design of LED-devices of the configuration ITO/PEDOT/polymer/Ca with improved parameters (η_{ext} = 2.15%, luminance = 5760 cd/m^2) relative to the octyloxy-substituted polymer **15a** (η_{ext} = 0.79%, luminance = 1406 cd/m^2). Despite the differences in the conjugation pattern between polymers **15** and polymers **17** [(−Ph−C≡C−Ph−C≡C−Ph−CH=CH−Ph−CH=CH−)$_n$], an identical chromophore system of structure Ph−C≡C−Ph−CH=CH−Ph−CH=CH−Ph−C≡C−Ph was found to be responsible for their emissive behavior as confirmed by fluorescence kinetics measurements (τ, k_f, k_{nr}) and quantum chemical calculations. The differences observed in their solid-state photophysical properties are ascribed to the combined effects of the backbone rigidity (as a function of the number of −C≡C− moieties in the repeating unit) and the nature of the side chains. Moreover less −C≡C− units within polymers **15** lead to the more than 100-fold improvement of their electroluminescent parameters compared to polymers **17**.

Introduction

The design and synthesis of soluble conjugated polymers are presently subject of great research interest, as a result of their wide range of applications in optoelectronic devices[1] such as light-emitting diodes (LEDs),[2] light-emitting electrochemical cells,[3] field effect transistors (FETs),[4] lasers,[5] and organic solar cells.[6] These materials have the advantage of a facile color tunability, good film-forming properties, and adequate mechanical properties in comparison to their inorganic counterparts.[1,7] Poly(phenylene−vinylene)s (PPVs) and their dehydrogenated congeners poly(phenylene−ethynylene)s (PPEs) are among the most widely studied π-conjugated polymers.[2a,7,8] With the aim to combine the interesting intrinsic properties of both classes of compounds into one polymeric material, our group and others designed alkyl- and/or alkoxy-substituted hybrid phenylene−vinylene/phenylene−ethynylene polymers (PPV−PPE)s of well-defined repeating units backbones (−Ph−C≡C−Ph−CH=CH−)$_n$ and (−Ph−C≡C−Ph−C≡C−Ph−CH=CH−Ph−CH=CH−)$_n$, **17**, corresponding to a 1 to 1 ratio of the −C≡C− and −CH=CH− moieties.[9,10]

The electronic and optical properties of conjugated polymers are controlled both by the primary molecular structure (intramolecular functionality: π-conjugation) and by the supramolecular organization (intermolecular interactions: π-stacking) in a similar way to that in which secondary and ternary structures are fundamental to the functions of proteins.[11,12] Control over the supramolecular interactions have been mainly implemented and mediated via the structural, chemical, and electronic properties of side chains.[12,13] Thorough investigations of the influence of the alkoxy side chains

* Corresponding authors. (D.A.M.E.) Telephone: (+49)-3641-948245. Fax: (+49)-3641-948202. E-mail: c5ayda@uni-jena.de. (T.P.) Telephone: (+49)-6131-379113. Fax: (+49)-6131-379100. E-mail: pakula@mpip-mainz.mpg.de.

† Institut für Organische Chemie und Makromolekulare Chemie der Friedrich-Schiller Universität Jena.

‡ Max-Planck-Institut für Polymerforschung.

§ University of Massachusetts.

⊥ Konarka Austria Forschungs-u. Entwicklungs GmbH.

|| Institut für Physikalische Chemie der Friedrich-Schiller Universität Jena.

10.1021/ma0488111 CCC: $27.50
Published on Web 09/08/2004

Scheme 1

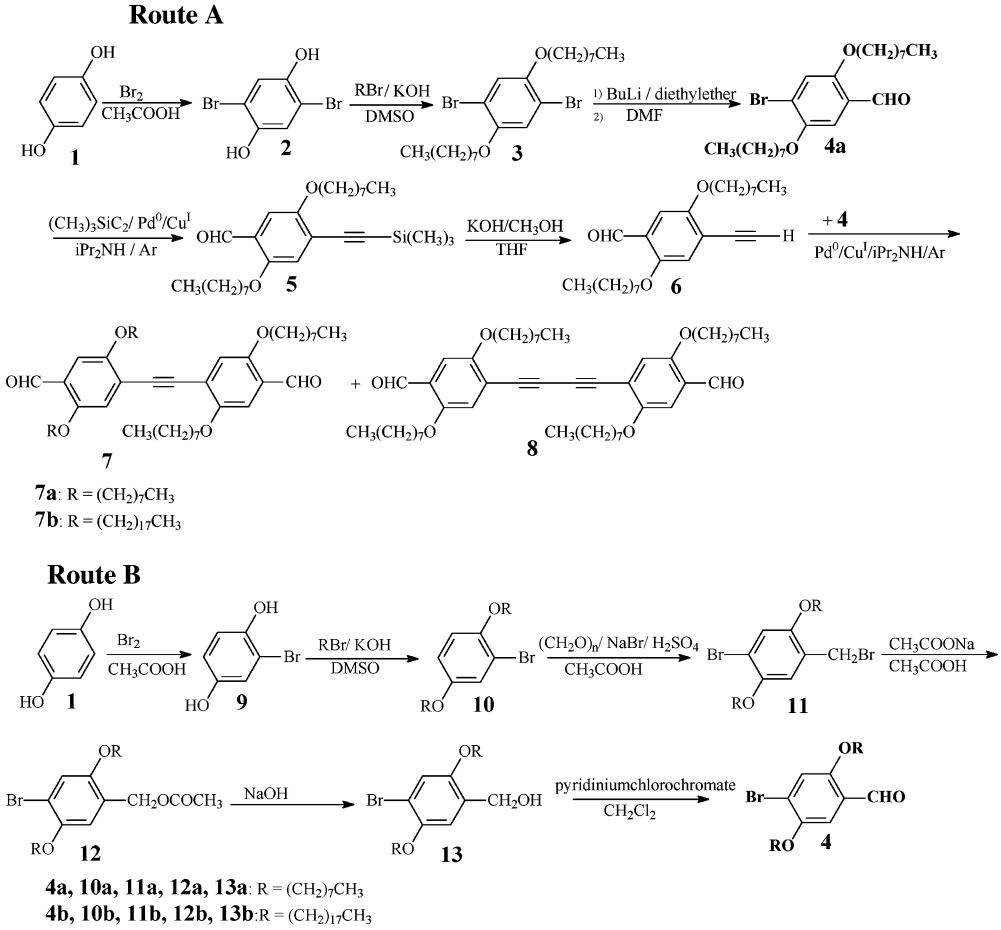

on the photophysical properties of polymers **17** have been previously reported.[10b,d] In this article, we report the synthesis and characterization of alkoxy-substituted yne-containing poly(phenylene−vinylene), **15a−d,** whose repeating units (RU), (−Ph−C≡C−Ph−CH=CH−Ph−CH=CH−)$_n$, incorporate −C≡C− and −CH=CH− moieties in a 1 to 2 ratio. Our synthetic strategy consisting of first applying the Sonogashira cross-coupling reaction[8] in combination with chromatographic work up to obtain pure monomeric dialdehyde **7** before proceeding with the Horner−Wadsworth−Emmons olefination reaction in the polycondensation process, using the synthetic and work up protocols as described elsewhere by us,[10] provides highly pure polymers deprived of diyne-defect structures. Alkoxy side chains of various length and geometry have been grafted on the phenylene−vinylene moieties of the polymers. What effect does macromolecular design (conjugation pattern within the backbone repeating unit (RU) and nature of side chains) have on the solid-state properties of the hybrid polymers **15a−d**? An attempt to give an answer to this question is the subject of this article, in which complementary analytical methods have been employed to account for the properties of the compact bulk materials. Thermal and phase behaviors were determined using thermogravimetric analysis (TGA), differential scanning calorimetry (DSC), and polarized optical microscopy (POM). The superstructure morphologies were established using small-angle light scattering (SALS) experiments, while assignment of the packing structure was documented by analysis of the 2D diffraction patterns recorded for uniaxially oriented specimens. Moreover the photophysical (absorption and emission in solution as well as in solid state, fluorescence kinetics in solution, electroluminescence (EL), and photoconductivity) and electrochemical properties of the new compounds have been investigated. The electrochemical data were determined through the combination of cyclic voltammetry (CV) and electrochemical voltage spectroscopy (EVS). Comparison of the photophysical properties of hybrid polymers **15** with those of hybrid polymers **17** revealed an identical π-conjugated pattern of structure Ph−C≡C−Ph−CH=CH−Ph−CH=CH−Ph−C≡C−Ph to constitute the effective chromophore system responsible for the emissive behavior of both classes of polymers. This was confirmed by solution fluorescence kinetics measurements and quantum chemical calculations. However reducing the number of −C≡C− units within the conjugated backbone from polymers **17** to polymers **15** is the source of more than 100-fold improvement of the EL parameters.

Results and Discussion

Synthesis and Characterization. The prerequisite for the synthesis of defect-free yne-containing poly(phenylene−vinylene)s **15** is the prior synthesis of fluorophoric dialdehyde **7** [1,2-bis(4-formyl-2,5-dialkoxyphenyl)acetylene]. The synthetic pathway to **7** is illustrated in Scheme 1. The most important component in this synthetic series is 4-bromo-2,5-dialkoxybenzaldehyde (**4**), which can be obtained through two synthetic routes. According to route A shown in Scheme 1, **4** is obtained in a three-step reaction from hydroquinone (**1**) as described elsewhere.[10d] The last step of this synthetic route, the Bouveault formylation[14] of 1,4-dibromo-2,5-dialkoxybenzene (**3**) using 1 equiv each of butyllithium

Scheme 2

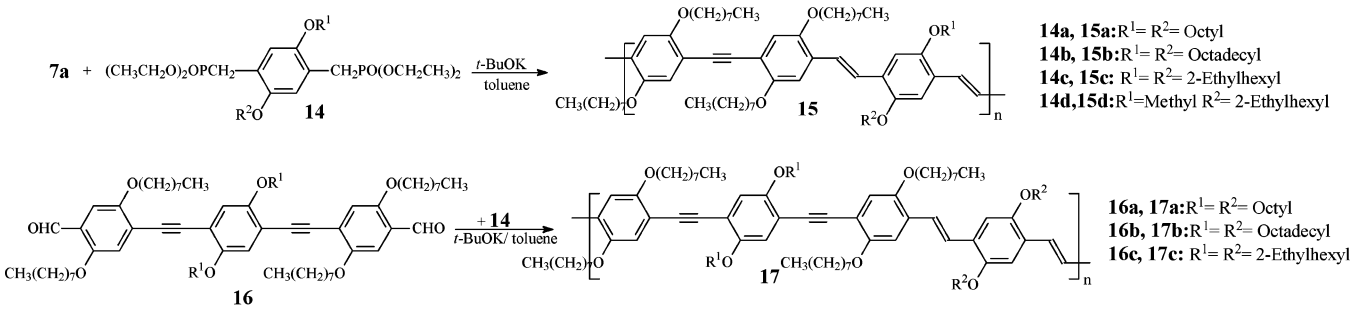

Table 1. Data from GPC (polystyrene as standard, THF as eluent)

code	$\bar{M}_n$	$\bar{M}_w$	$\bar{M}_z$	M_p	$\bar{M}_w/\bar{M}_n$	$\overline{DP}$
15a	7000	15 000	28 000	8000	2.1	7
15b	11 000	28 000	61 000	15 000	2.9	8
15c	7500	23 500	49 000	18 000	3.1	7
15d	8000	21 000	38 000	20 600	2.6	8

and dimethylformamide in diethyl ether while keeping the temperature as low as possible, is limited to compounds with side chains not longer than octyl, due to solubility problems at low temperature. Moreover many synthetic runs are needed to get a substantial amount of **4a** (4-bromo-2,5-dioctylbenzene) as a result of the said solubility problems. No side chain limitations are observed in the case of route B, which is a six-step reaction also starting from hydroquinone (**1**), thus allowing the synthesis for example of **4b** (4-bromo-2,5-dioctadecylbenzaldehyde).

The Sonogashira Pd-catalyzed cross coupling reaction[8] of **4a**,**b** with 1-ethynyl-4-formyl-2,5-dioctyloxybenzene (**6**)[10d] and subsequent chromatographic purification afforded **7a** (R = octyl) and **7b** (R = octadecyl) as yellow compounds in 52 and 74% yield, respectively, alongside a small amount of the diyne derivative **8** [1,4-bis(4-formyl-2,5-dioctyloxyphenyl)butadiyne-1,3]. The ^{13}C NMR spectra in deuterated chloroform of **7a** and **8** show identical peaks except the peaks of the acetylenic carbons, which are detected around 93 ppm in the case of **7a** and around 80 ppm in the case of **8** (See Supporting Information, Figures S1 and S2).

The Horner-Wadsworth-Emmons olefination reactions[15] of **7a** with various bisphosphonate esters **14a**−**d** afforded polymers **15a**−**d** as red materials in yields between 60 and 90% after work up (Scheme 2). The alkoxy side chains enable good solubility of the polymers in standard organic solvents, such as THF, toluene, chlorobenzene, DMSO, dichloromethane, and chloroform. The ^{13}C NMR spectra of **15c** and **15a**, for example, obtained in deuterated chloroform are shown in the Supporting Information as Figures S3 and S4, respectively. The chemical structures of the polymers were further confirmed through ^{1}H NMR, IR (KBr), and elemental analysis. Weight-average molecular weights, M_w, between 15 000 and 28 000 g/mol were obtained, showing polydispersity indices between 2.1 and 3.1 and degree of polymerization ($\overline{DP}$) between 7 and 8 (Table 1). The almost identical $\overline{DP}$ values for all four polymers are a prerequisite for a reliable comparison of their various properties.

Investigations in the Bulk. One of the goals of this study is to evaluate the effects of the structural features of yne-containing PPVs **15a**−**d** on their thermal behavior, morphology and structure in bulk. All along the following text polymer **15a** is referred as standard compound owing to its regular structure ($R^1 = R^2 =$ octyl). Polymers **15b** ($R^1 = R^2 =$ octadecyl), **15c** ($R^1 = R^2 =$ 2-ethylhexyl) and **15d** ($R^1 =$ methyl, $R^2 =$ 2-ethylhexyl) will respectively enable the emphasis of the effects of side chains extension, side chains geometry (branched vs linear) and a quasi removal of one side chain.

Thermal Analysis. TGA carried under air while heating at a rate of 10 K/min, shows that polymers **15** are thermostable up to temperatures of about 638 to 673 K, at which 5% weight loss was recorded. Thus, the polymers were handled comfortably without decomposition up to isotropization temperature. Figure 1 includes both sets of heating and cooling DSC curves for the four polymers. DSC thermograms of **15a** and **15b** have similar features exhibiting two reversible transitions with weak and broad peaks extended over 60 K for the lower temperature transition and over 90 and 130 K for the higher temperature transition of **15b** and **15a**, respectively. The higher temperature transitions were detected at slightly lower temperature on cooling. The lower temperature transition may be assigned to an order−disorder process of the side chains as previously reported for similar rigid-rod polymers having aromatic backbones substituted by alkyl side chains.[16] Compound **15c** is characterized by the presence of a unique reversible transition detected at temperatures of ∼500 and ∼470 K during the first and second heating runs, respectively. Upon cooling, an exothermic peak occurs in the temperature range between 463 and 363 K, which represents the crystallization of **15c** according to POM observations as will be shown later. Polymer **15d** showed two endotherms on first heating at 333 and 515 K while subsequent cooling and heating runs did not reveal clear transitions. Note that the DSC signals recorded during cooling of the four polymers were rather noisy, suggesting a heterogeneous crystallization process taking place.

Polarized Optical Microscopy. According to POM observations, the higher temperature transitions were detected as the temperatures at which the materials melt and enter into the isotropic phase. The optical micrographs for the **15d** sample taken during the first heating run at 10 K/min and observed under crossed polaroids are shown in Supporting Information Figure S5. The texture remains almost unchanged below 473 K. At this temperature, the color changes rapidly and finally the sample goes to an isotropic state when it is heated to 539 K. Upon cooling, the sample starts to show birefringence at 508 K, and its color changes and becomes reddish when it is cooled to a temperature of 473 K. Even at a temperature of 553 K, **15d** gives a highly viscous melt. Since **15d** has a molecular weight

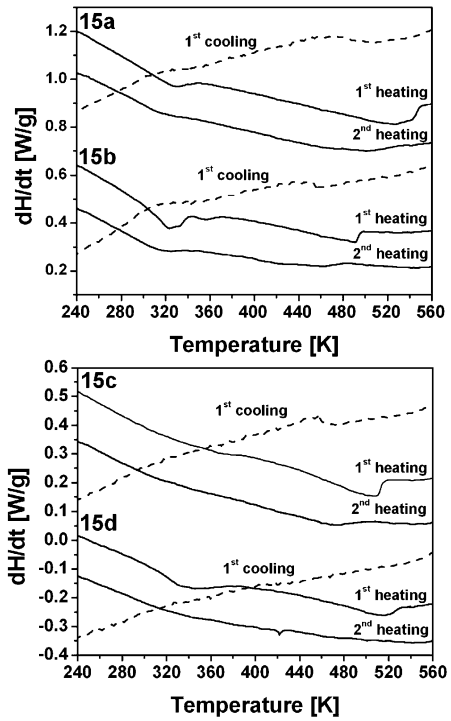

Figure 1. DSC traces recorded during heating (solid lines) and cooling (dashed lines) of **15a** and **15b** (top) and of **15c** and **15d** (bottom) at 10 K/min. Both the first and second heating cycles are shown.

comparable to that of **15a** and **15c** (Table 1), its high melt viscosity may be attributed to the fact that **15d** possesses the lowest number of side chain carbon atoms of the series, which may favor strong interactions between aromatic backbones.[17] Tendency to aggregate formation for **15d** was also evidenced through the investigation of solid-state photoluminescence and electroluminescence properties as will be shown later on.

Rather similar morphology changes were observed during first heating of **15a**, **15b**, and **15c**, while in such cases, first, flowing of polymer was evidenced when heated to isotropic state and, second, the appearance and growth of birefringent domains from the isotropic melt was identified as following nucleation and growth process. As an example, optical micrographs taken during cooling of **15a** at temperatures of 493 (left) and 303 K (right) are shown in Supporting Information Figure S6. It is seen that the color changes also upon cooling and the size of the birefringent domains is on the order of a few micrometers. POM observations at the early stage of the crystallization process have given the impression that **15a** leads to the formation of spherulite-like birefringent domains, while **15b** and **15c** give rise to elongated-shape birefringent structures.

Small-Angle Light Scattering. To further elucidate the morphology formation during crystallization, SALS experiments were performed for the samples as obtained after POM. *Hv* SALS patterns recorded for **15a**, **15b**, and **15c** polymers at room temperature exhibit a 4-fold symmetry but differ in the orientation of the lobes with respect to the polarization axes (Figure 2).

The pattern of **15a** confirms that spherulitic crystal morphology develops during cooling.[18] The nature of the scattering patterns obtained for **15b** and **15c** may be interpreted in terms of a supramolecular structure involving a rodlike aggregate of crystals which is anisotropic and which may not have correlated orientation in space.[19] Note that **15d** gave an azimuthal angle independent SALS pattern.

Powder Wide-Angle X-ray Pattern. The structure of yne-containing PPVs was initially characterized by means of wide-angle X-ray scattering on powder samples. Figure 3 gives azimuthally averaged X-ray scattered intensity distributions at room temperature for the four samples as obtained directly after polymerization (solid lines) and after being heated to isotropic state and then cooled to room temperature (dashed lines). Yne-containing PPVs give a major peak in the small-angle region reflecting a *d*-spacing of 1.51−2.2 nm. As shown in lower left part of Figure 3, diffractograms obtained from *as-polymerized* and *melt-crystallized* **15c** samples show a change of the position of the small-angle peak. This finding suggests the occurrence of two phases associated with different molecular packing and that the structure with the shortest *d*-spacing (largest S^{-1} value) is thermodynamically more stable. Polymers **15a**, **15b**, and **15c** give rise to several well-defined diffraction peaks in the wide-angle region superimposed to an amorphous halo suggesting they self-assemble into supramolecular organizations occurring due to spatial segregation between aromatic and aliphatic segments, stacking properties of π-conjugated main chains, and crystallization behavior of alkoxy side chains. Only an amorphous halo is seen in the wide-angle region of **15d** that originates from liquidlike intermolecular correlation and represents a broad distribution of intermolecular distances. These initial results confirm that both the structural features of polymer and thermal treatment may affect the self-organized supramolecular structure of yne-containing PPVs.

Fiber Wide-Angle X-ray Pattern. The polymers were processed at elevated temperatures by a microextrusion process allowing the preparation of macroscopically oriented specimens for their wide-angle X-ray structure analysis using a 2-dimensional detector.[20] The four specimens exhibit X-ray patterns showing strong equatorial reflections resulting from polymer backbones being extended along the fiber axis coinciding with the extrusion direction (Figure 4).

The fiber X-ray pattern of **15a** shows that regular macromolecules exhibit a more ordered structure via $\pi-\pi$ stacking of the aromatic rigid main chains and interactions of flexible alkyloxy side chains. The broad reflections along the equator at wide-angles give a distance of ∼0.42 nm characteristic of a side-to-side distance between aliphatic segments.[21] Polymer **15c** gives reflections in the low-angle region with two spacings $d_1 = 2.195$ nm and with $d_2 = 1.712$ nm. In the wide-angle amorphous halo two reflections at *d*-spacing of 0.477 and 0.388 nm are evident. This latter distance that is larger than the 0.335 nm sheet-to-sheet distance of graphite is consistent with the π-stacking correlation usually observed for π-conjugated macromolecular self-assemblies.[22−24] Polymers **15d** and **15b**, having side chains of different lengths, give rise to a wide-angle diffuse scattering halo corresponding to a liquidlike short-range order in molecular packing.

From the above results one can estimate that a probable structure adopted by yne-containing PPVs involves the formation of polymeric backbone layers, with the flexible alkoxy side chains filling the space between neighboring layers. The absence of repeating unit reflections along the meridian rules out correlation between neighboring polymeric backbones. In such a

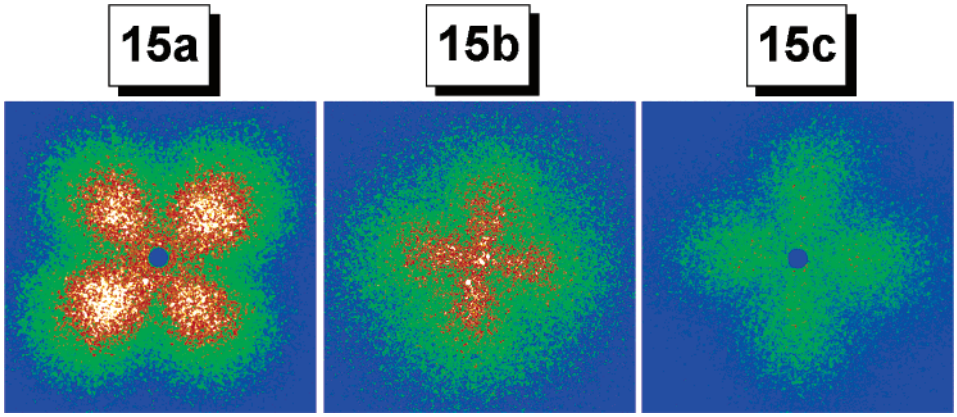

Figure 2. SALS *Hv* patterns for **15a**, **15b**, and **15c** taken at room temperature after cooling from isotropic melt.

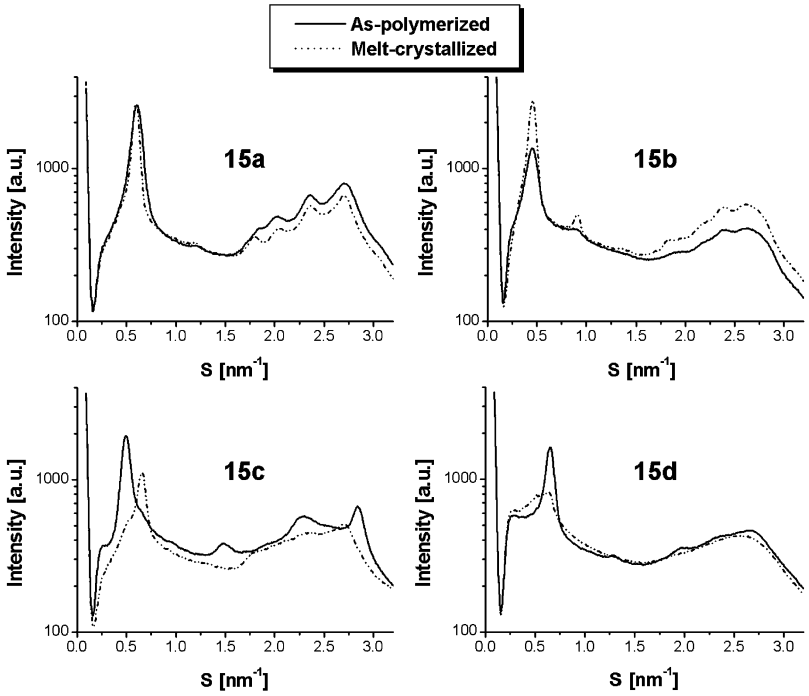

Figure 3. Powder wide-angle X-ray diffractograms of **15a**, **15b**, **15c**, and **15d** taken at room temperature for *as-polymerized* (solid line) and *melt-crystallized* (dashed lines) samples.

layered model, the space between the layers should be controlled by the volume fraction of the side chains.[25] Thus, the position of the maximum scattered intensity of the small-angle equatorial reflections is dependent on the molecular mass of the repeating unit (M^{RU}) and reflects the correlation between the axes of the backbone layers. As illustrated in Figure 5, this correlation scales with M^{RU} following a regression line whose slope is unity indicating 1-dimensional dependence of intermolecular distances with respect to the side chains volume fraction.

Extrapolation to the molecular mass of the repeat unit backbone gives a distance of ∼6 Å indicating monomolecular backbone layers to be formed. For comparison, values of *d*-spacing calculated for powder samples are also included in Figure 5. Typically, shorter layer spacings were obtained for the sample in powder form, meaning that the extrusion process leads to conformationally regular polymer chains with lower packing density in the lateral direction. The combination of alkoxy side chains differing in size (from methyloxy to octadecyloxy) and geometry (linear vs branched) may result in varied molecular structures so that it is difficult to ascertain a definite packing model. For instance, **15c** having the same number of carbon atoms in each side branches as **15a** leads to a slightly lower *d*-spacing value due to the presence of two branched side chains (2-ethylhexyloxy) while **15a** has solely linear octyloxy side chains. However, regarding **15a** as model polymer one can try to assign a packing structure. Assuming a π-stacked structure with end-to-end packing of fully extended octyloxy side chains, **15a** gives an increment of 1.13 Å per carbon atom (considering the oxygen as a methylene group), which is lower than the predicted value of 1.25 Å/CH_2.[21] This finding suggests a tilt angle of about 65° of the alkoxy side chains with respect to the polymer backbone axis.

Temperature-Dependent Fiber Wide-Angle X-ray Pattern. Azimuthally averaged scattering intensity distributions for **15c** filament taken at selected temperatures during heating (H) and subsequent cooling (C) are presented in Supporting Information Figure S7. Upon heating, the small-angle reflections corresponding to the d_1-spacing decrease in intensity and disappear above 353 K together with the 0.388 nm *d*-spacing reflections related to the interchain distance within the

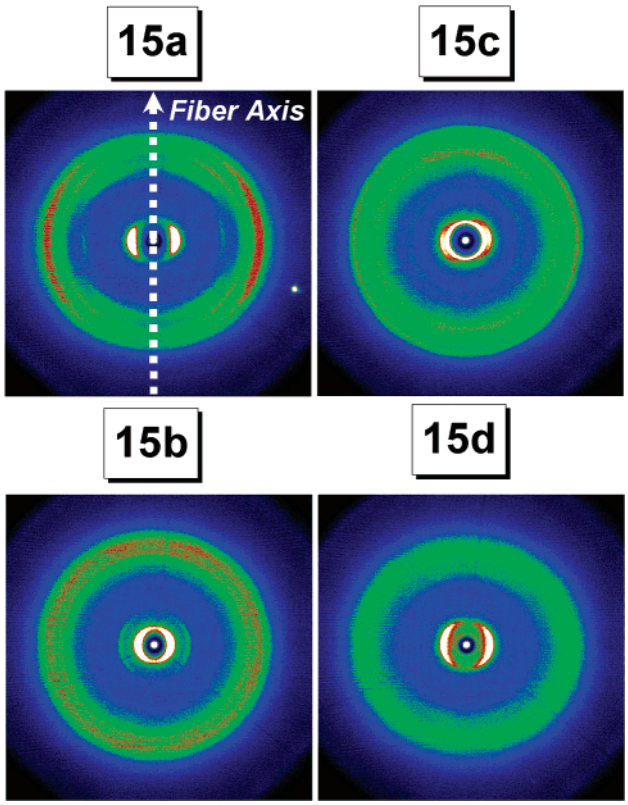

Figure 4. 2D wide-angle X-ray diffraction fiber patterns from oriented specimens of **15a**, **15b**, **15c**, and **15d** taken at room temperature after extrusion. The arrow indicates the direction of the fiber axis.

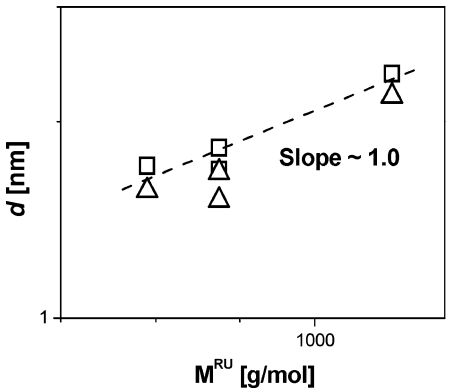

Figure 5. Layer spacing observed by 2D wide-angle X-ray fiber patterns at room temperature as a function of the molecular mass of the repeating unit (M^{RU}) for extruded fibers (□) and powder samples (△).

layers. From a temperature of 383 K, the intensity of the small-angle reflections corresponding to the d_2-spacing is greatly enhanced. Upon cooling, the reflection in the wide-angle region is shifted to a smaller 2θ value and appears much more broader, indicating that finite disorder is maintained within the layers, while in the small-angle region the reflections reminiscent of the d_1-spacing do not reappear below 353 K so that the layered structure with the denser lateral packing is thermodynamically more stable, in agreement with the X-ray powder analysis. The two structures reminiscent of the d_1- and d_2-spacing developed according to thermal treatment and owing to extrusion at elevated temperature are both present in the *as-extruded* specimen. Diffraction patterns and corresponding scattering intensity distributions obtained for **15d** and **15b** in

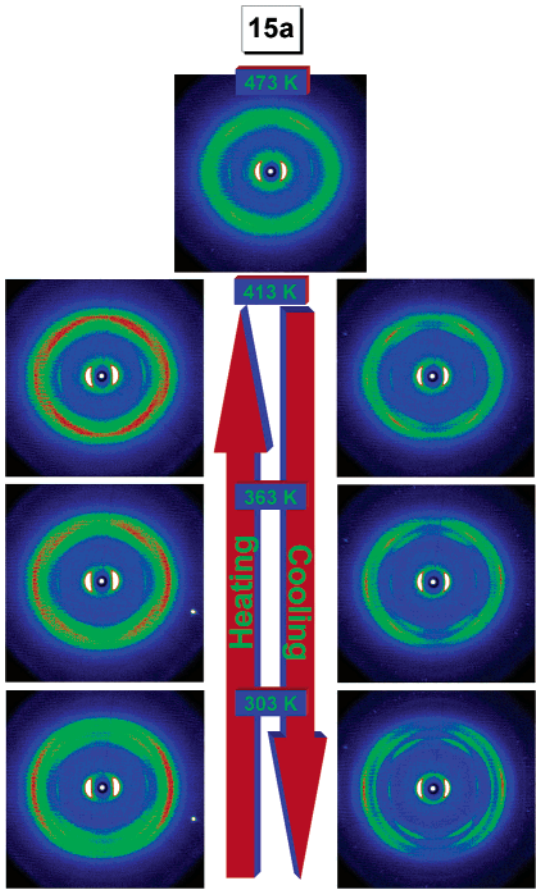

Figure 6. 2D wide-angle X-ray diffraction fiber patterns of an oriented sample of **15a** during heating and subsequent cooling at temperatures of 303, 363, 413, and 473 K.

oriented form did not show any significant changes with temperature. Typically, higher orders of the small-angle reflections appear upon cooling suggesting a better ordering in the direction perpendicular to the polymer backbone, while a diffuse scattering halo is maintained in the wide-angle region. Polymer **15a** was found to be more sensitive to thermal treatment as shown by the 2D wide-angle X-ray patterns presented in Figure 6. The reflections in the wide-angle region narrow and show increased intensities up to a temperature of 413 K, above which they almost disappear with the sharp, intense layer reflections remaining only. Further heating brings a shift of the amorphous halo to a lower 2θ value. Upon cooling, beginning from 413 K, redistribution of the intensities in the wide-angle region is observed, since azimuthally distributed meridional reflections indicating correlation distances of about 0.46 and 0.54 nm clearly show up with increased intensity upon further cooling. Besides these eight off-meridional reflections, two more reflections attributed to the short-range inter-side chains distance show up along the equator from a temperature of 363 K, which corroborates the results of DSC analysis (Figure 1). These findings indicate a rearrangement of the aromatic planes of the PPV structural unit during annealing of **15a**.

Photoconductivity. Photoconductivity is among the potential functionalities arising from conjugated compounds.[10,26−29] The photoconductivity spectra are shown in Figure 7. The maximum photocurrents of the compounds, I_{ph}, (difference between total current in the presence of light and the dark current) are given in

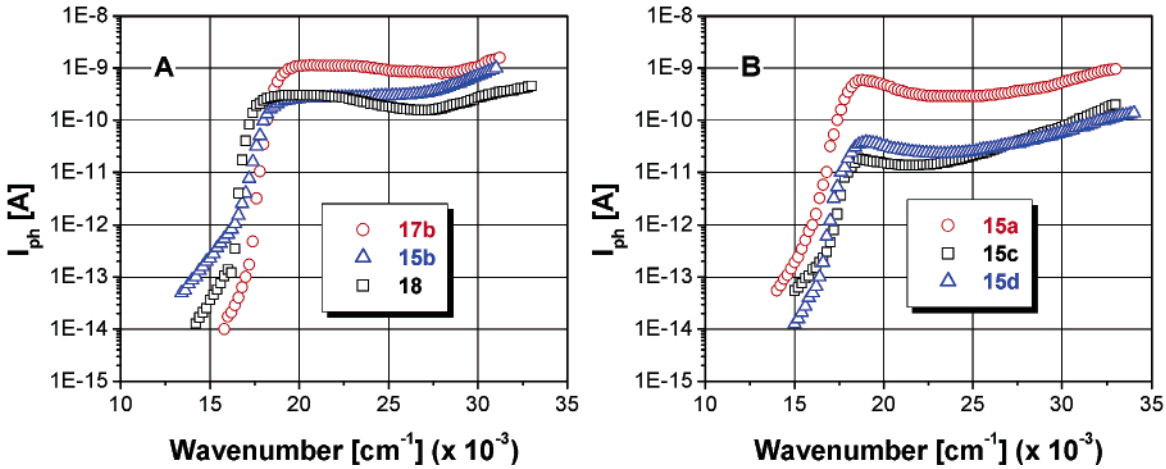

Figure 7. Photoconductivity spectra of polymers **15a**−**d**, **17b**, and **18** (surface type cell, slit width 0.2 mm, threshold voltage 10 (A) or 20 V (B)).

Table 2. Data from Photoconductivity Studies

code	voltage (V)	I_{Ph}[a] (A)	ν_{max}[b] (cm^{-1})
15a	20	5.9×10^{-10}	18 800
15b	10	3.0×10^{-10}	20 000
15c	20	1.7×10^{-11}	18 600
15d	20	3.8×10^{-11}	19 000
17b	10	1.1×10^{-9}	20 000
18	10	3.0×10^{-10}	20 000

[a] Maximum photocurrent. [b] Wavenumber of irradiating light at I_{Ph}.

Table 2. I_{ph} values of order 10^{-11} and 10^{-10} A at wavenumbers between 18 000 and 20 000 cm^{-1} were obtained for **15a**−**d**; however the applied voltage necessary for the detection of photoconductivity is side chain dependent. A voltage of 20 V was required to detect photoconductivity in the cases of polymers **15a**, **15c**, and **15d** having short side chains. Comparatively lower voltage (10 V) was necessary in the case of **15b** having longer octadecyloxy side groups. This is in agreement with our previous observations for polymers **17b** and **18** [poly(1,4-(2,5-dioctadecyloxy)phenylene−vinylene-1,4-(2,5-dioctyloxy)phenylene−vinylene] (for the chemical structure see Supporting Information Figure S8) having same longer side chains.[10e] The synthesis of polymers **17a**−**c** is illustrated in Scheme 2. They were obtained from dialdehydes **16a**−**c** under the same reaction conditions as described here for the synthesis of polymers **15a**−**d**.[10d]

Absorption and Photoluminescence Investigations. The photophysical characteristics of the hybrid polymers **15a**−**d** and **17a**−**c** along with the dialdehydes **7**, **8** and **16** were investigated by UV−vis absorption and photoluminescence measurements in dilute chloroform solution as well as in solid state. Fluorescence kinetics measurements in solution and quantum chemical calculations were carried out to substantiate the conclusions derived from the comparison of the properties of both classes of polymers.

The absorption maxima, λ_a, the extinction coefficients at the maximum wavelength, ϵ_{max}, the optical energy gaps, E_g^{opt}, the emission maxima, λ_f, the Stokes shifts, and the fluorescence quantum yields, ϕ_f, are presented in Table 3 and Supporting Information Table S9.[10d] Table 4 summarizes data from the kinetics measurements, namely fluorescence lifetime, τ, fluorescence rate constant, k_f, the rate constant of radiationless deactivation, k_{nr}, the fluorescence rate constant according to Strickler and Berg, k_f(SB),[30] and the ratio between k_f and k_f(SB).

Table 3. Data from UV−Vis Absorption and Photoluminescence Investigations in Solution and in the Solid State

code	λ_a (nm)	ϵ_{max}[c] ($M^{-1}.cm^{-1}$)	E_g^{opt} (eV)	λ_f[d] (nm)	Stokes shift[e] (nm (cm^{-1}))	ϕ_f[f] (%)
7a[a]	410	22 100	2.79	457	47 (2510)	50
7b[a]	409	30 700	2.69	452	43 (2330)	49
8[a]	411	30 990	2.72	452	41 (2210)	41
16a[a]	423	57 060	2.61	468	45 (2270)	65
15a[a]	472	60 200	2.36	524	52 (2100)	70
15a[b]	491		2.17	*556*, 593	65 (2380)	19
15b[a]	473	67 560	2.34	525	52 (2090)	78
15b[b]	492		2.18	*557*, 596	65 (2370)	28
15c[a]	475	65 500	2.34	528	53 (2110)	72
15c[b]	484	-	2.21	*554*, 593	70 (2610)	38
15d[a]	474	53 040	2.34	525	51 (2050)	64
15d[b]	492	-	2.19	601	109 (3690)	17

[a] Solution. [b] Solid state. [c] Per mole of the repeating unit in the case of the polymers. [d] Italicized data indicate the major peak. [e] $\lambda_f - \lambda_a$ ($1/\lambda_a - 1/\lambda_f$). [f] Fluorescence quantum yield, ± 10%.

Table 4. Fluorescence Lifetime in Dilute Chloroform Solution and Rate Constants of the Deactivation Processes

code	τ[a] (ns)	k_f[b] (ns^{-1})	k_f(SB)[c] (ns^{-1})	k_f/k_f(SB)	k_{nr}[d] (ns^{-1})
7a	1.85	0.27	0.21	1.3	1.85
7b	1.90	0.26	0.29	0.9	1.98
8	1.50	0.27	0.27	1.0	2.16
16a	1.44	0.45	0.51	0.9	0.76
15a	0.77	0.91	0.48	1.9	0.33
15b	0.76	1.03	0.52	2.0	0.21
15c	0.71	1.01	0.52	2.0	0.28
15d	0.74	0.86	0.41	2.1	0.42
17a	0.74	0.99	0.56	1.8	0.27
17b	0.76	1.12	0.68	1.6	0.13
17c	0.76	0.97	0.84	1.2	0.27

[a] Fluorescence lifetime, ±0.05 ns. [b] Fluorescence rate constant: $k_f = \phi_f/\tau$; ϕ_f values from Table 3 and Supporting Information Table S9. [c] Fluorescence rate constant according Strickler and Berg:[30] k_f (SB) $= 2.88 \times 10^{-9} \times n^2 \times \int F(\nu)/\nu^3 \, d\nu / \int F(\nu) \, d\nu \times \int \epsilon(\nu)/\nu \, d\nu$, n = refractive index of the solvent, $F(\nu)$ = corrected fluorescence spectrum. [d] Rate constant of radiationless deactivation: $k_{nr} = (1 - \phi_f)/\tau$.

Solution absorption and emission spectra of the monomeric dialdehydes **7a**,**b**, **8**, and **16a** and polymers **15a** and **17a** can be viewed in Figures 8 and 9, respectively. Compounds **7** and **8** exhibit similar absorption maxima at around 410 nm. The differences lie within the shorter wavelength part of their spectra

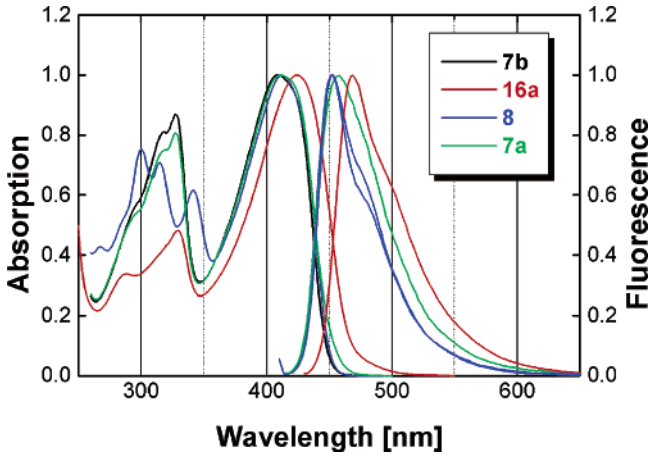

Figure 8. Absorption and emission spectra of dialdehydes **7a**,**b**, **8**, and **16** in dilute chloroform solution.

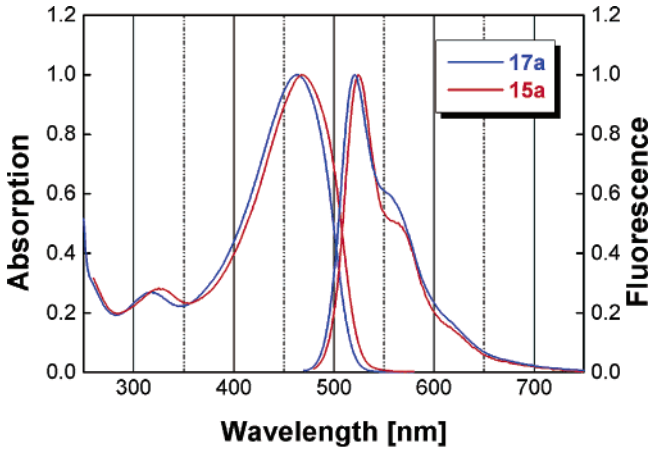

Figure 9. Absorption and emission spectra of polymers **15a** and **17a** in dilute chloroform solution.

between 250 and 350 nm, where the diyne-containing dialdehyde **8** shows a highly structured band. The larger chromophore system in **16a** compared to **7a** explains the ca. 10 nm bathochromic shift of its absorption (423 nm) and emission (468 nm) and the higher absorption coefficient. While **7a** emits at 457 nm, the emission maximum of **7b** at $\lambda_f = 452$ nm is 5 nm blue shifted. $\lambda_f = 452$ nm is also the emission maximum of dialdehyde **8**. The fluorescence quantum yields of **7**, **8** and **16a** are high with values of 50, 40, and 65%, respectively. The radiative rate constants k_f of the monomers, determined with ϕ_f and τ and according to Strickler and Berg are in good accordance, indicating that the emissive state is the same as the primarily populated one and geometrical changes between S_0 and S_1 states are negligible.

Despite the differences in the conjugation pattern, polymers **15** and **17** show almost identical photophysical behavior in dilute chloroform solution (Figure 9, Table 3, and Supporting Information Table S9). Only a slight bathochromic shift of the absorption and emission of polymers **15a**−**d** ($\lambda_a = 472-475$ nm, $\lambda_f = 524-528$ nm, $E_g^{opt} = 2.34$ eV), having one phenylene−ethynylene unit in the RU less than polymers **17a**−**c** ($\lambda_a = 468-470$ nm, $\lambda_f = 519-521$ nm, $E_g^{opt} = 2.37$ eV), is observed. That gives evidence of an identical chromophore system responsible for the emission in both types of polymers. This is moreover confirmed by the kinetic measurements. As well the fluorescence lifetimes τ as the radiative rate constants k_f of the different polymers are

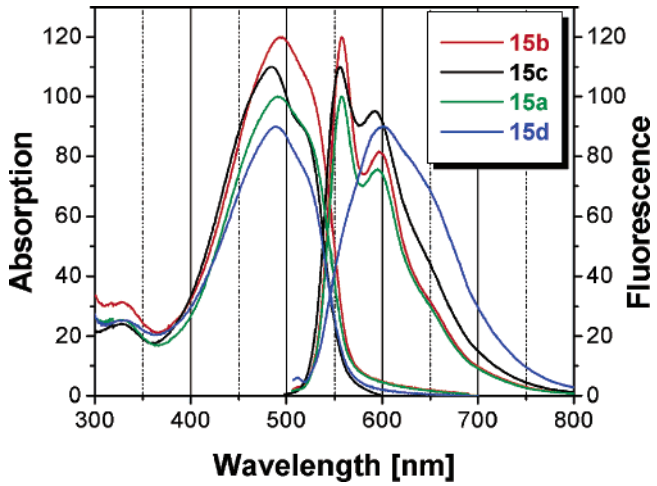

Figure 10. Solid-state absorption and emission spectra of polymers **15a**−**d**.

practically the same. The difference in the radiative rate constants k_f(SB) is due to the used absorption coefficients which are determined per repeating unit of the polymer. The RU's do not correspond to the effective chromophore segment. From the relation of the rate constants k_f/k_f(SB) (Table 4), we conclude an effective chromophore system extending over approximately two RU's in the case of polymers **15** or 1.5 RU's in the case of polymers **17** having an absorption coefficient twice as large as the given value for polymers **15** or 1.5 times higher than the given value for polymers **17** (Table 3 and Supporting Information Table S9).

We assume the effective fluorophore segment located around the lower energy phenylene−vinylene units of the compounds and having the structure Ph−C≡C−Ph−CH=CH−Ph−CH=CH−Ph−C≡C−Ph as shown in Chart 1. This assumption is moreover confirmed by quantum chemical calculations[31] performed with a series of different segments of the polymer backbone in order to localize the regions where π-conjugation is most effectively restricted and also to guide the selection of the most appropriate model compound (Chart 2). Alkoxy side groups were replaced by OH groups to simplify the calculations. The essential outcome is: If there are two consecutive *p*-phenylene−ethynylene moieties linked to two consecutive *p*-phenylene−vinylene units as described here, then π-conjugation extends only over one *p*-phenylene−ethynylene unit; it drops down rapidly over two units. We are led to this conclusion from a comparison of the rotational barriers between aromatic rings linked by ethynylene moieties which are, for instance 7.5 kJ/mol for **DM1** and 1.9 and 3.8 kJ/mol for the outer phenyl ring alone while the phenylene−ethynylene−phenylene unit is kept coplanar in **DM3**, respectively. The same conclusion is drawn from the inspection of the HOMO's and LUMO's which insignificantly extend over more than one consecutive phenylene−ethynylene unit. The isodensity contour maps of the HOMO and LUMO of **DM1** and **DM3** are depicted in Supporting Information Figure S10.

The solid-state absorption and emission spectra of polymers **15** are depicted in Figure 10. For the purpose of comparison, those of polymers **17** are shown in Supporting Information Figure S11.[10d] The differences in the solid-state emission curves are related to the various aggregation modes due to the combination of conjugation pattern and nature of grafted alkoxy side

Chart 1. Blue-Labeled Portion Considered as Chromophore System Responsible for the Emission

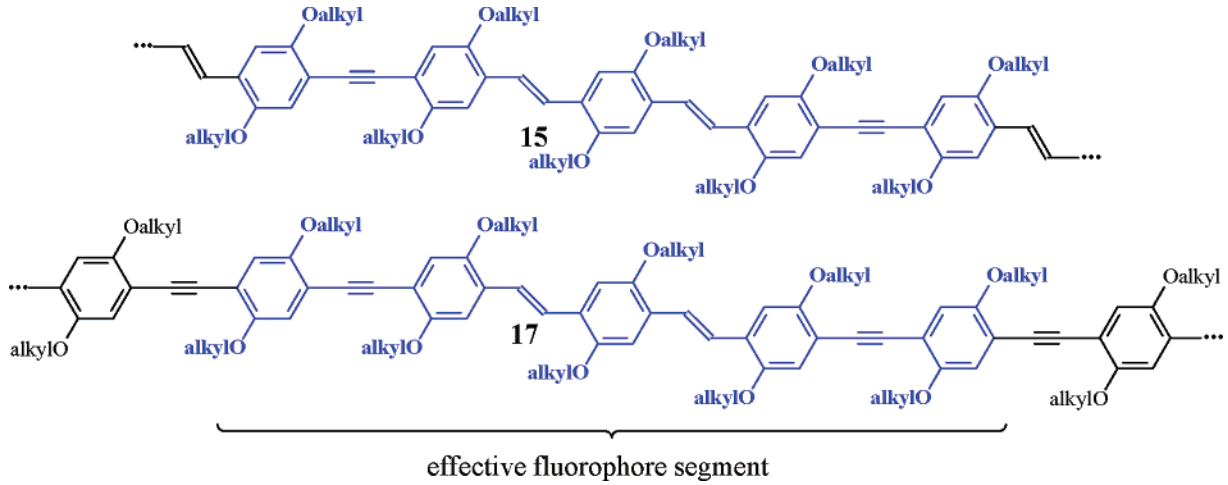

Chart 2. Rotational Energy Barrier as Obtained from Quantum Chemical Calculations

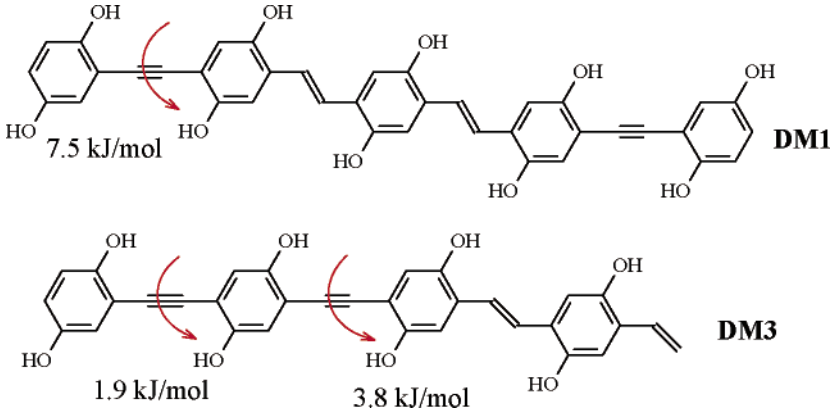

Table 5. Comparison of Electrochemical Data[a] of 15a−d with Those of MDMO−PPV[31e]

code	E^{ox}_{peak} (mV)	E^{red}_{peak} (mV)	E^{ox}_{onset} (mV)	E^{red}_{onset} (mV)	HOMO (eV)	LUMO (eV)	E_g^{ec} (eV)	$E_g^{ec} - E_g^{opt}$ (eV)
15a	∼+1000	−2010	+565	−1725	−5.32	−3.03	2.29	0.12
15b		∼−1980	+665	−1765	−5.42	−2.99	2.43	0.25
15c		∼−2000	+740	−1695	−5.49	−3.06	2.43	0.22
15d	+885	−1930	+645	−1725	−5.4	−3.03	2.37	0.18
MDMO−PPV	+670		+510	−1750	−5.26	−3	2.26	0.14

[a] All potential values are shown vs NHE; NHE-level used for HOMO−LUMO calculation was −4.75 eV.[33]

chains. The enhanced planarisation of the conjugated backbone in the solid state explains the red shift of the absorption ($E_g^{opt} \approx 2.20$ eV) and emission spectra relative to the solution. The grafting of methoxy group in **15d** leads to strong $\pi-\pi$ interactions (aggregates formation) and excimers formation, which explains its broad (full-width at half-maximum, $fwhm_f = 3400\ cm^{-1}$) and structureless emission curve peaked at $\lambda_f = 601$ nm, leading to the comparatively large Stokes shift of 109 nm ($\approx 3700\ cm^{-1}$) and the lowest fluorescence quantum yield of 17% among polymers **15**.

The effect of the conjugation pattern is clearly observed while comparing polymers **15a** and **17a**, both carrying octyloxy side groups in all phenyl rings. Enhanced rigidity due to the higher number of −C≡C− units in **17a**, compared with **15a**, and consequently enhanced $\pi-\pi$ interactions and excimer formation in the S_1 state result in a less structured and broad emission spectrum ($fwhm_f = 3400\ cm^{-1}$) and a large Stokes shift of 109 nm ($3800\ cm^{-1}$) and the lowest ϕ_f value of 23% among polymers of type **17**. The less rigid polymer **15a** as well as all polymers of type **15** and **17** consisting of either the branched bulky 2-ethylhexyloxy (**15c** and **17c**) or longer linear octadecyloxy (**15b** and **17b**) side chains is characterized with well structured emission curves made up of two maxima. The 0−0 transitions are centered around 552−559 nm and 0−1 transitions around 592−596 nm for all the above-mentioned polymers except polymer **17c**, where the steric hindrance due to bulky 2-ethylhexyloxy side chains is the source of the ca. 10 nm blue shift of its emission peaks located at 542 and 582 nm. Stokes shifts and $fwhm_f$ values between 2100 and 2600 cm^{-1} and fluorescence quantum yields between 30 and 50% were obtained for **15a−c** and **17b−c**, clearly indicating less aggregates/excimers contribution in the emissive process compared to **15d** and **17a**.

Electrochemical Investigations. The electrochemical behavior of the polymers was investigated by the combination of cyclic voltammetry (CV) and electrochemical voltage spectroscopy (EVS).[32] The corresponding data are given in Table 5.

Figure 11 depicts the cyclic voltammetry curves of **15a−d**. The dotted lines indicate the onset potentials as determined by EVS. The energy diagram presenting the position of the HOMOs and LUMOs is shown in the

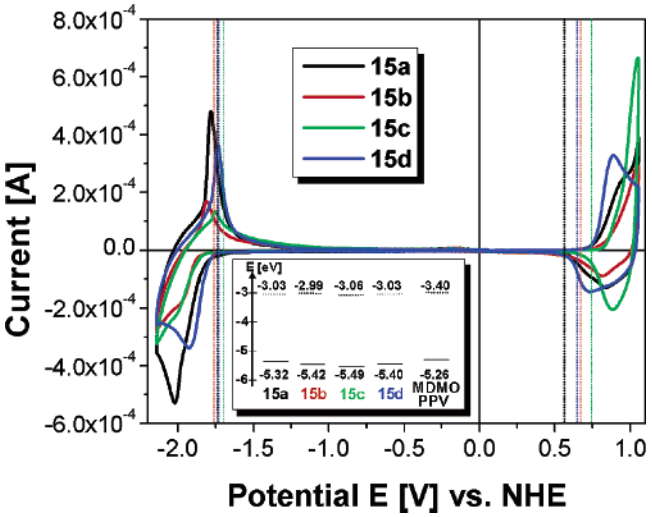

Figure 11. Cyclovoltammograms of **15a**−**d** recorded at 10 mV/s scan speed; the dotted lines indicate the onset potentials for the polymers according to the color code. The inset displays the position of the HOMO and LUMO of polymers **15a**−**d** and **MDMO**−**PPV** in the energy scale.

inset of Figure 11. All polymers exhibited partial reversibility in both n-doping and p-doping processes. Bulky substituents seem to disturb the conjugation[33] as the HOMO levels are lowered. Consequently **15c** with two branched 2-ethylhexyloxy substituents shows the lowest HOMO energy[34] of −5.49 eV. This effect is also strong but in a reduced form in the case of **15b** with longer linear octadecyloxy side groups, where a HOMO energy value of −5.42 eV was obtained; it reduces when one 2-ethylhexyloxy group is replaced by a methyloxy group in the case of **15d** (E_{HOMO} = −5.4 eV). Consequently the electrochemical band gap energies of both **15b** and **15c** at E_g^{ec} = 2.43 eV show a discrepancy of 0.25 and 0.22 eV to their respective E_g^{opt} values. The discrepancy of 0.12 eV in the case of polymer **15a** lies within the range of error. For the purpose of comparison the electrochemical data of poly[2-methoxy-5-(3′,7′-dimethyloctyloxy)-1,4-phenylene−vinylene] (**MDMO**−**PPV**)[32e] (for the chemical structure see Supporting Information Figure S8) are also given in Table 5. The higher oxidation potential onset values of polymers **15** compared with **MDMO**−**PPV** are evidence of enhanced oxidation stability due to the presence of −C≡C− units in **15**.

Electroluminescent Properties. Figure 12 shows EL spectra of ITO/PEDOT/polymer/Ca LEDs using polymers **15a**−**d**. The device from **15d** gives yellow light at 584 nm at 13 V. Other three devices emit green light at 547−557 nm. All the EL spectra display blue shift with increasing the applied voltage. For **15d** LED, when increasing the voltage from 13 to 21 V, the EL peak moves from 584 to 565 nm with a 19 nm blue shift. For **15b** LED, at 6 V, the EL spectrum shows two peaks at 552 and 593 nm, which correspond to 0−0 and 0−1 vibrational transitions respectively, similar to the PL spectrum. With voltage increase, the EL spectra show a blue shift, and the relative intensity of the 0−0 band continues to increase at the expense of the 0−1 band. LEDs using **15c** and **15a** show similar behavior. This indicates that the vibrational structure of the EL spectrum is sensitive to the applied electrical field. The EL blue shift under higher applied voltage is related to heating in the LEDs, which results in a thermochromic effect.[35] Band gap distributions in the polymers also contribute to the effect. The EL spectra of **15a**, **15b**, and **15c** LEDs show two bands while **15d** LED gives only one broad emission band. The small −OCH_3 group on the PV units gives more chance for polymer **15d** to form excimers compared with other three samples totally grafted with long side chains. The excimer emission will broaden the EL spectrum and also lead to a red shift.

Table 6. Electroluminescent Properties for ITO/PEDOT/Polymer/Ca Devices

code	λ_{max}^{EL} (nm)[a]	η_{ext} (%)	luminance (cd/m^2)
15a	*557*, 587 (6V)	0.79	1406
15b	*552*, 593 (6V)	2.15	5760
15c	*551*, 583 (10V)	1.82	1483
15d	*584* (13V)	0.22	595
17b	*543*, 581 (12V)	0.017	27.9[10e]

[a] Italicized data indicate the major peak.

Figure 13 shows the current density−voltage−luminance characteristics for the LEDs. The turn-on voltages for LEDs of **15d**, **15c**, **15a**, and **15b** are 7, 4, 3.5, and 5 V, respectively. The external quantum efficiencies reach 0.22, 1.82, 0.79, and 2.15% respectively. From **15d** to **15c** and from **15a** to **15b**, with increasing side chain length, the EL efficiency increases remarkably. The longer side chains will improve polymer solubility, film-forming capability, and film morphology which affect device performance significantly. In addition, longer side chains can form tiny domains to inhibit exciton interchain migration thus improving exciton confinement and EL efficiency.[36] Our previous study[36] indicates that polymers with grafted 2-ethylhexyloxy side chains are more efficient than those with grafted octyloxy side chains. In this work, **15c** shows higher efficiency than **15a**, conforming with previous results very well. 2-Ethylhexyloxy side chains may be more favorable for exciton confinement. There is more than a 100-fold improvement of the EL parameters from polymer **17b**[10e] to polymer **15b**, which can be ascribed to less −C≡C− units within compound **15b** compared to **17b** (Table 6).

Conclusions

Defect-free alkoxy-substituted yne-containing poly(phenylene−vinylene)s of general structure (−Ph−C≡C−Ph−CH=CH−Ph−CH=CH−)$_n$, **15a**−**d**, have been synthesized and characterized. A degree of polymerization around 7 was obtained for all the polymers enabling a reliable comparison of their properties as a function of the length and geometry of the grafted side chains. Formation of crystalline superstructures of either spherulitic-like (**15a**) or rodlike (**15b** and **15c**) morphology was identified as following typical nucleation and growth process for polymer having a symmetric substitution pattern. A layered structure consisting of π-stacked main-chain layers and the flexible alkoxy side chains occupying the space between is proposed for all the studied polymers. The discrepancy between the electrochemical (E_g^{ec}) and optical (E_g^{opt}) band gaps was found to be proportional to the bulkiness of the side chains. The presence of −C≡C− units within the polymers backbone constitutional unit enhances the oxidation stability of yne-containing PPVs **15** relative to MDMO−PPV. Octadecyloxy side chains in **15b** are not only required for the easy detection of the photoconductivity but also for the design of LED devices of configuration ITO/PEDOT/polymer/Ca with (comparatively to **15a**) improved parameters (η_{ext} = 2.15%, luminance = 5760 cd/m^2). These parameters are more

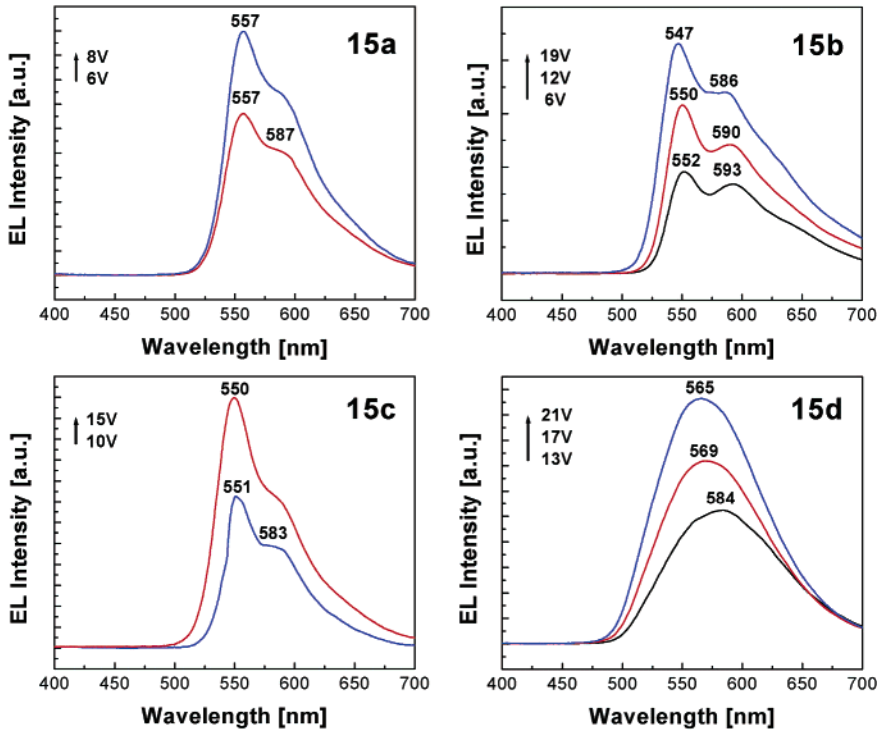

Figure 12. Electroluminescence spectra of **15a**−**d** from ITO/PEDOT/polymer/Ca devices.

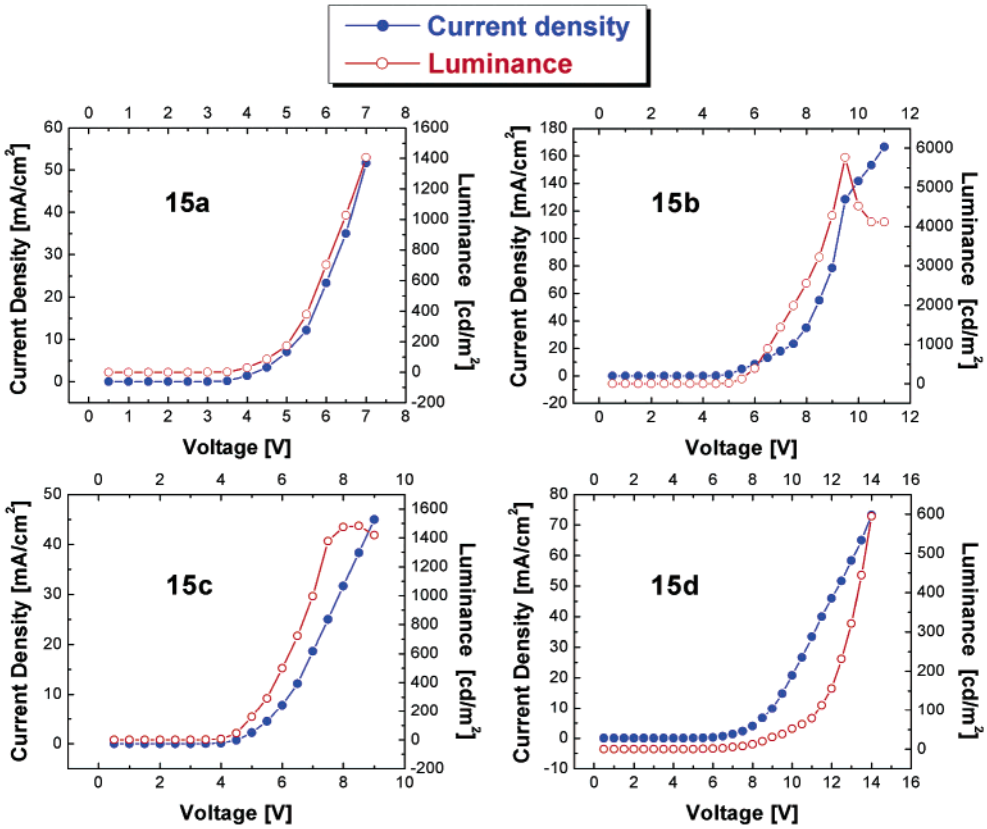

Figure 13. Current density−voltage (●) and luminance−voltage (○) characteristics for ITO/PEDOT/polymer/Ca devices from polymers **15a**−**d**.

than a 100-fold better than those of polymer **17b** due to less −C≡C− units within **15b**. Comparison of the photophysical properties of polymers **15** and polymers **17** as well as their corresponding monomeric dialdehydes **7** and **16** were carried out in dilute chloroform solution. Despite the differences in the conjugation pattern, an identical chromophore system, located around the lower energy portion of the polymers and having the structure Ph−C≡C−Ph−CH═CH−Ph−CH═CH−Ph−C≡C−Ph, is responsible for the emissive behavior of the both types of compounds. This is moreover confirmed by fluorescence kinetics measurements (τ, k_f,

k_{nr}) and quantum chemical calculations. The similarities or differences in solid-state emissive behavior of **15** and **17** result from the combination of backbone rigidity (as a function of the number of −C≡C− moieties in the repeating unit) and nature of side chains (length, geometry). The high absorption coefficients and high fluorescence quantum yields in the solid state combined with the enhanced oxidation stability (relative to PPV) make polymers **15a**−**d** potential donor materials in the design of organic solar cells.[37]

Acknowledgment. L.D. and F.E.K. wish to thank the AFOSR for generous financial support.

Supporting Information Available: Text describing the experimental procedures, the synthesis of the materials, and the characterization of the materials, Figures S1−S4, showing ^{13}C NMR spectra of **7a**, **8**, **15c**, and **15a**, Figures S5 and S6, showing POM observations for thin films of polymers **15c** and **15a**, Figure S7, showing X-ray diffractograms of **15**c, Figure S8, showing structures of **18** and MDMO−PPV, Table S9 showing UV−vis and photoluminescence data, Figure S10, showing isodensity contour maps of **DM1** and **DM3**, and Figure S11, showing solid state absorption and emission spectra of polymers **17a**−**c**. This material is available free of charge via the Internet at http://pubs.acs.org.

References and Notes

(1) (a) Hadziioannou, G., van Hutten, P. F., Eds. *Semiconducting Polymers: Chemistry, Physics and Engineering*, 1st ed.; Wiley-VCH: Weinheim, Germany, 2000. (b) Denton, F. R.; Lahti, P. M. In *Electrical and Optical Polymers*; Wise, D. L., Wnek, G. E., Trantolo, D. J., Cooper, T. M., Gresser, J. D., Eds.; Marcel Dekker: New York, 1998; p 61.

(2) (a) Kraft, A.; Grimsdale, A. C.; Holmes, A. B. *Angew. Chem., Int. Ed.* **1998**, *37*, 402. (b) Friend, R. H.; Gymer, R. W.; Holmes, A. B.; Burroughes, J. H.; Marks, T. N.; Taliani, C.; Bradley, D. D. C.; Dos Santos, D. A.; Brédas, J. L.; Lögdlund, M.; Salaneck, W. R. *Nature* **1999**, *397*, 121. (c) Schmitz, C.; Pösch, P.; Thelakkat, M.; Schmidt, H.-W.; Montali, A.; Feldman, K.; Smith, P.; Weder, C. *Adv. Funct. Mater.* **2001**, *11*, 41. (d) Pschirer, N. G.; Miteva, T.; Evans, U.; Roberts, R. S.; Marshall, A. R.; Neher, D.; Myrick, M. L.; Bunz, U. H. F. *Adv. Mater.* **2001**, *13*, 2691. (e) Sarker, A. M.; Gürel, E. E.; Ding, L.; Styche, E.; Lahti, P. M.; Karasz, F. E. *Synth. Met.* **2002**, *132* (3), 227.

(3) Pei, Q.; Yu, G.; Zhang, C.; Yang, Y.; Heeger, A. J. *Science* **1995**, *269*, 1086.

(4) Katz, H. E.; Bao, Z.; Gilat, S. L. *Acc. Chem. Res.* **2001**, *34*, 359.

(5) (a) Pauck, T.; Hernnig, R.; Perner, M.; Lemmer, U.; Siegner, U.; Mahrt, R. F.; Scherf, U.; Müllen, K.; Bässler, E. O.; Göbel, E. O. *Chem. Phys. Lett.* **1995**, *244*, 171. (b) Hide, F.; Diaz-Garcia, M. A.; Schwartz, B. J.; Andersson, M. R.; Pei, Q.; Heeger, A. J. *Science* **1996**, *273*, 1833.

(6) (a) Brabec, C. J.; Sariciftci, N. S.; Hummelen, J. C. *Adv. Funct. Mater.* **2001**, *11*, 15. (b) Piok, T.; Brands, C.; Neyman, P. J.; Erlacher, A.; Soman, C.; Murray, M. A.; Schroeder, R.; Graupner, W.; Heflin, J. R.; Drake, A.; Miller, M. B.; Wang, H.; Gibson, H.; Dorn, H. C.; Leising, G.; Guzy, M.; Davis, R. M. *Synth. Met.* **2001**, *116*, 343.

(7) *Handbook of Conducting Polymers*, 2nd ed.; Skotheim, T. J., Elsenbaumer, R. L., Reynolds, J. R., Eds.; Marcel Dekker: New York, 1998.

(8) Bunz, U. H. F. *Chem. Rev.* **2000**, *100*, 1605.

(9) (a) Brizius, G.; Pschirer, N. G.; Steffen, W.; Stitzer, K.; zur Loye, H.-C.; Bunz, U. H. F. *J. Am. Chem. Soc.* **2000**, *122*, 12435. (b) Bunz, U. H. F. *Acc. Chem. Res.* **2001**, *34*, 998. (c) Ramos, A. M.; Rispens, M. T.; van Duren, J. K. J.; Hummelen, J. C.; Janssen, R. A. J. *J. Am. Chem. Soc.* **2001**, *123*, 6714. (d) Schenning, A. P. H.; Tsipis, A. C.; Meskers, S. C. J.; Beljonne, D.; Meijer, E. W.; Brédas, J. L. *Chem. Mater.* **2002**, *14*, 1362. (e) Wilson, J. N.; Windscheif, P. M.; Evans, U.; Myrick, M. L.; Bunz, U. H. F. *Macromolecules* **2002**, *35*, 8681. (f) Chu, Q.; Pang, Y.; Ding, L.; Karasz, F. E. *Macromolecules* **2003**, *36*, 3848. (g) Tong, M.; Sheng, C. X.; Yang, C.; Vardeny, Z. V. *Phys. Rev. B* **2004**, *69*, 155211.

(10) (a) Egbe, D. A. M.; Tillmann, H.; Birckner, E.; Klemm, E. *Macromol. Chem. Phys.* **2001**, *202*, 2712. (b) Egbe, D. A. M.; Roll, C. P.; Birckner, E.; Grummt, U.-W.; Stockmann, R.; Klemm, E. *Macromolecules* **2002**, *35*, 3825. (c) Egbe, D. A. M.; Birckner, E.; Klemm, E. *J. Polym. Sci., Part A: Polym. Chem.* **2002**, *40*, 2670. (d) Egbe, D. A. M.; Bader, C.; Nowotny, J.; Günther, W.; Klemm, E. *Macromolecules* **2003**, *36*, 5459. (e) Egbe, D. A. M.; Bader, C.; Klemm, E.; Ding, L.; Karasz, F. E.; Grummt, U.-W.; Birckner, E. *Macromolecules* **2003**, *36*, 9303. (f) Zhokhavets, U.; Goldhahn, R.; Gobsch, G.; Al-Ibrahim, M.; Roth, H.-K.; Sensfuss, S.; Klemm, E.; Egbe, D. A. M. *Thin Solid Films* **2003**, *444*, 215. (g) Egbe, D. A. M.; Stockmann, R.; Hotzel, M. *J. Opt. A: Pure Appl. Opt.* **2004**, *6*, 791.

(11) Bucknall, D. G.; Anderson, H. L. *Science* **2003**, *302*, 1904.

(12) Cacialli, F.; Samori, P.; Silva, C. *Mater. Today* **2004**, *4*, 24.

(13) (a) Levitsky, I. A.; Kim, J.; Swager, T. M. *Macromolecules* **2001**, *34*, 2315. (b) Perahia, D.; Traiphol, R.; Bunz, U. H. F. *Macromolecules* **2001**, *34*, 151. (c) Weder, C.; Wrighton, M. S.; Spreiter, R.; Bosshard, C.; Günter, P. *J. Phys. Chem.* **1996**, *100*, 18931.

(14) Meier, H.; Aust, H. *J. Prakt. Chem.* **1999**, *341*, 466.

(15) Pfeiffer, S.; Hörhold, H.-H. *Macromol. Chem. Phys.* **1999**, *200*, 1870.

(16) (a) Ballauff, M. *Makromol. Chem., Rapid Commun.* **1986**, *7*, 407. (b) Rodriguez-Parada, J. M.; Duran, R.; Wegner, G. *Macromolecules* **1989**, *22*, 2507.

(17) (a) Majnusz, J.; Catala, J. M.; Lenz, R. W. *Eur. Polym. J.* **1983**, *19*, 1043. (b) Krigbaum, W. R.; Hakemi, H.; Kotek, R. *Macromolecules* **1985**, *18*, 965.

(18) (a) Stein, R. S.; Rhodes, M. B. *J. Appl. Phys.* **1960**, *31*, 1873. (b) Stein, R. S. *Structures and Properties of Polymer Films*, Lenz, R. W., Stein, R. S., Eds.; Plenum: New York, 1973 (c) Samuels, R. J. *J. Polym. Sci., Part A-2*, **1971**, *9*, 2165.

(19) (a) Stein, R. S.; Erhardt, P.; van Aartsen, J. J.; Clough, S.; Rhodes, M. *J. Polym. Sci., Part C* **1966**, *13*, 1.

(20) Andreopoulou, A. K.; Carbonnier, B.; Kallitsis, J. K.; Pakula, T. *Macromolecules* **2004**, *37*, 3576.

(21) (a) Swan, P. R. *J. Polym. Sci.* **1962**, *56*, 403. (b) Jordan, E. F.; Feideisen, D. W.; Wrigley, A. N. *J. Polym. Sci., Part A-1* **1971**, *9*, 1835. (c) Hsieh, H. W.; Post, B.; Morawetz, H. *J. Polym. Sci., Polym. Phys. Ed.* **1976**, *14*, 1241.

(22) (a) Winokur, M. J.; Wamsley, P.; Moulton, J.; Smith, P.; Heeger, A. J. *Macromolecules* **1991**, *24*, 3812. (b) McCullough, R. D.; Tristram-Nagle, S.; Williams, S. P.; Loewe, R. D.; Jayaraman, M. *J. Am. Chem. Soc.* **1993**, *115*, 4910. (c) McCullough, R. D.; Ewbank, P. C.; Loewe, R. S. *J. Am. Chem. Soc.* **1997**, *119*, 633.

(23) (a) Chen, T.-A.; Rieke, R. D. *J. Am. Chem. Soc.* **1992**, *114*, 10087. (b) Wu, X.; Chen, T.-A.; Rieke, R. D. *Macromolecules* **1995**, *28*, 2101. (c) Chen, T.-A.; Wu, X.; Rieke, R. D. *J. Am. Chem. Soc.* **1995**, *117*, 233.

(24) (a) Yamamoto, T. *Chem. Lett.* **1996**, 703. (b) Yamamoto, T.; Komarudin, D.; Arai, M.; Lee, B.-L.; Suganuma, H.; Asakawa, N.; Inoue, Y.; Kubota, K.; Sasaki, S.; Fukuda, T.; Matsuda, H. *J. Am. Chem. Soc.* **1998**, *120*, 2047. (c) Yamamoto, T.; Suganuma, H.; Maruyama, T.; Inoue, T.; Muramatsu, Y.; Arai, M.; Komarudin, D.; Ooba, N.; Tomaru, S.; Sasaki, S.; Kubota, K. *Chem. Mater.* **1997**, *9*, 1217. (d) Yamamoto, T.; Oguro, D. *Macromolecules* **1996**, *29*, 1833. (e) Morikita, T.; Yamaguchi, I.; Yamamoto, T. *Adv. Mater.* **2001**, *13*, 1862. (f) Yamamoto, T.; Lee, B.-L. *Macromolecules* **2002**, *35*, 2993.

(25) (a) Ballauf, M.; Schmidt, G. F. *Mol. Cryst. Liq. Cryst.* **1987**, *147*, 163. (b) Ballauf, M.; Schmidt, G. F. *Makromol. Chem., Rapid. Commun.* **1987**, *8*, 93. (c) Watanabe, J.; Harkness, B. R.; Sone, M. *Polym. J.* **1992**, *24*, 1119. (d) Kloppenburg, L.; Jones, D.; Claridge, J. B.; zur Loye, H.-C.; Bunz, U. H. F. *Macromolecules* **1999**, *32*, 4460.

(26) Law, K.-Y. in *Organic Conductive Molecules and Polymers*; Nalwa, H. S., Ed.; John Wiley & Sons Ltd.: West Sussex 1997; Vol. 1. p 487.

(27) Funahashi, M.; Hanna, J. I. *Phys. Rev. Lett.* **1997**, *78*, 2184.

(28) Kim, S.; Park, S. Y. *Macromolecules* **2001**, *34*, 3947.

(29) You, W.; Cao, S.; Hou, Z.; Yu, L. *Macromolecules* **2003**, *36*, 7014.

(30) Strickler, S. J.; Berg, R. A. *J. Chem. Phys.* **1962**, *37*, 814.

(31) The fully optimized geometry was obtained from density functional theory calculations using b31yp/6−31 g(d) functional implemented in the GAUSSIAN98 package [Frisch, M. J.; et al. Gaussian98 (revision A7), Gaussian Inc.: Pittsburgh, PA, 1989]. The barriers are giving the differences between

the total energies of the coplanar and 90° twisted conformations, that means, they do not contain thermal and zero-point energy corrections.

(32) (a) Kaufmann, J. H.; Chung, T.-C.; Heeger, A. J. *J. Electrochem. Soc.* **1984**, *131*, 2847. (b) Eckhardt, H.; Shacklette, L. W.; Yen, K. Y.; Elsenbaumer, R. L. *J. Chem. Phys.* **1989**, *91*, 1303. (c) Mühlbacher, D.; Neugebauer, H.; Cravino, A.; Sariciftci, N. S.; van Duren, J. K. J.; Dhanabalan, A.; van Hal, P. A.; Janssen, R. A. J.; Hummelen, J. C. *Mol. Cryst. Liq. Cryst.* **2002**, *385*, 205. (d) Mühlbacher, D.; Cravino, A.; Neugebauer, H.; Sariciftci, N. S. *Synth. Met.* **2003**, *137*, 1361. (e) Mühlbacher, D. Diploma thesis on Comparative Study of the Electrochemical and Optical Band Gap of Organic Semiconductors. Johann Kepler University, Linz, Austria, 2002.

(33) Liu, B.; Yu, W.-L.; Lai, Y.-H.; Huang, W. *Chem. Mater.* **2001**, *13*, 1984.

(34) (a) Gomer, R. J.; Tryson, G. *J. Chem. Phys.* **1977**, *66*, 4413. (b) Kötz, R.; Neff, H.; Müller, K. *J. Electroanal. Chem.* **1986**, *215*, 331.

(35) (a) Braun, D.; Heeger, A. J. *Appl. Phys. Lett.* **1991**, *58*, 1982. (b) Braun, D.; Moses, D.; Zhang, C.; Heeger, A. J. *Appl. Phys. Lett.* **1992**, *61*, 3092.

(36) Ding, L.; Egbe, D. A. M.; Karasz, F. E. *Macromolecules* **2004**, *37*, 6124.

(37) Sensfuss, S.; Al-Ibrahim, M.; Konkin, A.; Nazmutdinova, G.; Zhokhavets, U.; Gobsch, G.; Egbe, D. A. M.; Klemm, E.; Roth, H.-K. *Proc. SPIE* **2004**, *5125*, 129.

MA0488111